Available online at www.sciencedirect.com
ScienceDirect
Journal of Nuclear Materials 375 (2008) 113–119
journal of nuclear materials
www.elsevier.com/locate/jnucmat

Quantum mechanical calculations of uranium phases and niobium defects in γ-uranium

Shikai Xiang [a], Hanchen Huang [a,*], L.M. Hsiung [b]

[a] Department of Mechanical, Aerospace and Nuclear Engineering, Rensselaer Polytechnic Institute, Troy, New York 12180, USA
[b] Lawrence Livermore National Laboratory, Chemistry, Materials, and Life Sciences Directorate, P.O. Box 808, L-352, Livermore, CA 94551, USA

Received 12 November 2007; accepted 15 November 2007

Abstract

Depleted uranium (U) from fuel enrichment processes has a variety of applications due to its high density. With the addition of a small concentration of niobium (Nb), U becomes stainless. Nb is fully miscible with the high-temperature γ phase of U and tends to segregate upon cooling below 1050 K. The starting point of segregation is the configuration of Nb substitutional or interstitial defects. Using quantum mechanical calculations, the authors find that the formation energy of a single vacancy is 1.08 eV, that of Nb substitution 0.59 eV, that of Nb interstitial at octahedral site 1.58 eV, and that of Nb interstitial at tetrahedral site 2.35 eV in the dilute limit of isolated defects; all with reference to a reservoir of the pure γ phase U and pure Nb. The analysis of electronic structures reveals the correlation of formation energies of Nb defects with the local perturbations of electron distribution. Higher formation energy of Nb defects correlates with larger perturbation. Based on this study, Nb atoms thermodynamically prefer to occupy substitutional sites in the γ phase U.

PACS: 61.72.Ji; 61.66.Dk

1. Introduction

Uranium (U) is known to exist in three solid phases: α, β and γ [1,2]. Even in the nuclear materials community, U is relatively less commonly investigated and literature on U is relatively rarer. We therefore will first briefly describe the atomic arrangements in these three phases; as shown in Fig. 1. The α phase has an orthorhombic structure, and its conventional unit cell contains four atoms, as in face-centered-cubic (fcc) crystals Fig. 1(a). However, the atoms at sites J and K are not at face centers although they are on front and back faces. Further, there are no atoms on the left and right faces; instead, one effective atom, labeled L, resides inside the unit cell [3]. The crystal structure of β (Fig. 1(b)) and γ (Fig. 1(c)) phases are body-centered-tetragonal (bct) and body-centered-cubic (bcc), respectively. The bct structure is deformed bcc, so the periodicity along vertical direction is different from those along the horizontal directions. Under ambient pressure, the α, β and γ phases are stable at 0–940 K, 940–1050 K and 1050–1407 K, respectively [1].

Depleted U containing little ^{235}U may be the by-product of enrichment or from spent fuels of fission reactors. Such depleted U has found a variety of applications. With a density of 19 kg/m^3, U is 70% denser than lead and slightly less dense than tungsten [4]. Because of the high density, bullets or projectiles made of U can be small in size; one advantage of the smallness is the reduction of aerodynamic drag. For the same reason, tank armors made of U are resistant to projectiles [5]. In the form of pure solid, U is prone to oxidation. The addition of small amount of Nb significantly improves its corrosion resistance, allowing the production of 'stainless' U. Together with Zr, the addition of Nb to

* Corresponding author. Tel.: +1 518 276 2020; fax: +1 518 276 6025.
E-mail address: hanchen@rpi.edu (H. Huang).

0022-3115/$ - see front matter © 2007 Elsevier B.V. All rights reserved.
doi:10.1016/j.jnucmat.2007.11.003

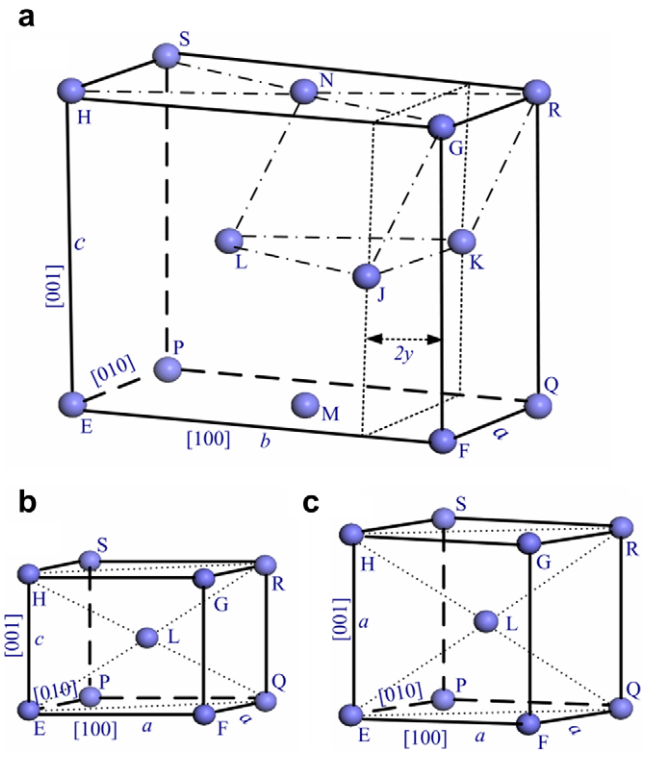

Fig. 1. Crystal structures of (a) α, (b) β, and (c) γ phases, with U atoms shown as spheres and directions shown by Miller indices. The *a*, *b*, *c* and *y* are lattice constants, and atomic labels (such as P and M) are for reference later on.

U also stabilizes the γ phase at low temperature [6] for applications as metallic fuel [7,8]. Due to the low solubility of Nb in α and β phases of U, Nb is introduced to the high-temperature γ phase [9,10]. This paper examines where Nb atoms sit as they are introduced into the high-temperature γ phase.

Density functional theory based quantum mechanical calculations offer a reliable tool to investigate Nb defects in U. For small simulation cells, appropriate for perfect crystal calculations, full-potential all-electron calculations lead to reliable results of lattice constants [11,12], elastic constants [13], charge density wave (CDW) [14], and high temperature and high pressure phase diagram [2]. Once defects are involved, large simulation cells are necessary and the calculations are based on pseudopotentials. Such calculations of point defects in uranium oxide [15] and uranium nitride [16] have proven reliable in terms of lattice constants of perfect crystal and defects formation energies.

Using the same pseudopotential of Ref. [16], this paper investigates Nb defects in γ phase of U. In Section 2, we describe the computational details. Section 3 has two components. In the first component, we report relative stabilities and electronic structures of α, β, and γ phases of U. In the second component, we report formation energies and electronic structures near a vacancy, an Nb substitutional or an interstitial defect in γ phase of U. Finally, in Section 4 we summarize the conclusions.

2. Computational method

Within the framework of density functional theory, we perform all the calculations with plane-wave bases using the projector augmented wave (PAW) method, as implemented in Vienna ab initio simulations package (VASP) [17,18]. The standard PAW potentials in VASP include $6s^2 6p^6 5f^3 6d^1 7s^2$ valence electrons for U and $4p^6 5s^1 4d^4$ for Nb. The partial densities of state, which are based on Mulliken population analysis [19], show that inclusion of these valence electrons is sufficient. We use GGA descriptions for exchange-correlation [20] and set the cutoff energy in plane-wave basis expansion as 350 eV for both U and Nb. Use of a larger cutoff of 400 eV leads to variation of vacancy formation energy within 0.02 eV and that of elastic constant within 0.3%. We use Methfessel and Paxton's Fermi-level smearing method (width = 0.2 eV) to accelerate electronic structure relaxation [21]. Using perfect crystals as test cases, we show that exclusion of spin–orbit interactions causes a negligible error, at least for β and γ phases. Therefore, calculations involving defects do not include spin–orbit interactions, for better computational efficiency. All the geometric relaxations follow a quasi-Newton algorithm using the exact Hellmann–Feynman forces, with a convergence criterion of force being 0. 1 eV/nm.

In determining the equilibrium structures of pure U, we use the primitive cell with periodic boundary conditions. The *k*-point meshes are $20 \times 20 \times 26$, $24 \times 24 \times 22$, and $26 \times 26 \times 26$ for α, β and γ phases, respectively. For the perfect crystal of bcc Nb, we also use the primitive cell with periodic boundary conditions, and use *k*-point mesh of and $26 \times 26 \times 26$. When the mesh density increases up to $30 \times 30 \times 30$ for all the four cases, the energy variations are within 1 meV/atom. For the α and β phases, which have internal freedom in the primitive unit cells, cell shape and ion positions also relax. The starting configuration of the cell shape and internal freedom is based on experimental values [3]. In rigorous calculations, an elastic constant should be the curvature near equilibrium lattice constants [22]. However, in order to compare with existing quantum mechanical calculation and experimental data of bulk modulus and its pressure derivative, we adopt the third-order Birch–Murnaghan equation of state [23]. The variation of bulk modulus from these two calculation methods is within 1%.

In the study of defects in the γ phase of U, we use larger simulation cells with periodic boundary condition. Three types of defect configurations are: single vacancy, Nb at substitutional site, and Nb at interstitial site. The size of simulation cell (which is also called supercell) is $3 \times 3 \times 3$ in the unit of bulk lattice constant a; the cell contains 54 lattice sites. Use of larger cell of $4 \times 4 \times 4$ containing 128 lattice sites leads to variation of vacancy formation energy within 0.05 eV. The *k*-point meshes are $6 \times 6 \times 6$, and other parameters are the same as for pure U calculations. When the *k*-point mesh density increases up to $8 \times 8 \times 8$,

the variation of vacancy formation energy is within 0.01 eV.

Turning to defect formation energies, we consider the dilute limit of isolated defects. As a reference point, the energy of each isolated atom at ground state is zero. The formation energy of a single vacancy E_v is defined as

$$E_v = E_{(n-1)U} - \frac{(n-1)}{n} E_{nU}, \quad (1)$$

where $E_{(n-1)U}$ is the total energy of $(n-1)$U atoms in a simulation cell of n lattice sites, and E_{nU} is the total energy of a perfect U cell containing nU atoms; the empty lattice site represents a vacancy. The formation energy of an Nb substitutional defect E_s is defined as

$$E_s = E_{(n-1)U+Nb} - \frac{(n-1)}{n} E_{nU} - E_{Nb}, \quad (2)$$

where $E_{(n-1)U+Nb}$ is the total energy of $(n-1)$U atoms and one Nb atoms occupying the n lattice sites of a simulation cell, and E_{Nb} is the total energy of each Nb in a perfect bcc crystal. The formation energy of Nb interstitial defect E_I is defined as

$$E_I = E_{nU+Nb} - E_{nU} - E_{Nb}, \quad (3)$$

where E_{nU+Nb} is the total energy of nU atoms occupying the n lattice sites and one Nb atom occupying an interstitial site of a simulation cell. To facilitate comparison of the calculation results with their experimental counterpart, we note that the definition here assumes pure bcc Nb and pure γ phase of U as sources and sinks in defect formation.

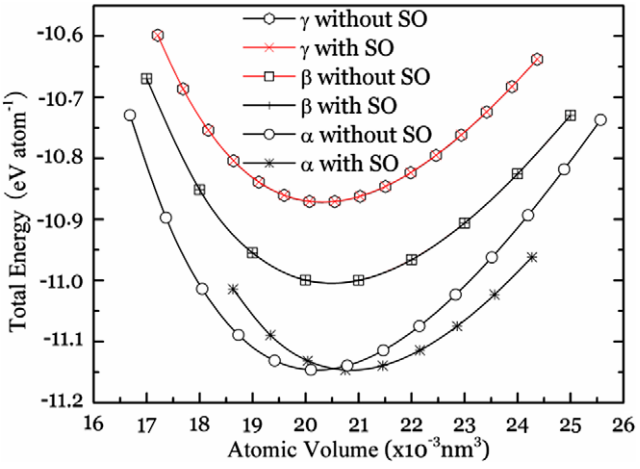

Fig. 2. Total energy versus atomic volume for α, β and γ phases of U; with or without spin–orbit (SO) interactions.

3. Results

In this section, we start from results of pure U, and proceed to those of the γ phase of U containing a vacancy or an Nb defect, using the former for comparison and contrast. In order to test the validity of the computational method, we first determine the total energy as a function of atomic volume. From this function, we may derive equilibrium lattice constants, bulk moduli, and their derivatives with respect to pressure for the α, β and γ phases. Shown in Fig. 2 is the total energy as a function of atomic volume, with and without spin–orbit interactions. Consistent with experimental observation [1], the α phase is more stable than the γ phase at 0 K. For comparison, Table 1 lists our results of the α phase with (PAW+w) and without (PAW+wt) spin–orbit interactions and literature data. The data include available experimental measurements [2,3] and two versions of full-potential-based (FP) calculation results with spin–orbit interactions; one using linear muffin-tin orbital (LMTO) [13] and the other using linear augmented plane wave (LAPW) [24]. The experimental measurements of lattice constants are at 4 K, and the modulus at room temperature. The lattice constants from our calculations with spin–orbit interactions are in agreement with experimental values within about 1%. Our results of lattice constants are also comparable to other quantum mechanical calculation results by similar margin, and elastic constants by about 7% [13]. These comparisons indicate that the general method used here is reasonable.

Fig. 2 also reveals another interesting feature, relevant to spin–orbit interactions. With or without spin–orbit interactions, the energy dependence on atomic volume remains almost the same for bother β and γ phases. When it comes to the γ phase, which is the focus of this study, our calculations without spin–orbit interactions show that the bulk modulus is 122.6 GPa and its pressure derivative is 4.1; these compare well with the experimental values of 113.3 GPa and 3.4 [2]. These results show that the PAW and GGA together can reproduce the experimental results for pure U, without spin–orbit interactions.

Beyond the energy–volume relationships, electron distributions provide further insights to atomic bonding in U. As the density of state (DOS) in Fig. 3 shows, the 6s and

Table 1
Properties of the α phase: Atomic volume V in unit of nm^3, lattice constants (a, b, c, and y) in unit of nm, bulk modulus B in unit of GPa and its pressure derivative B′

	V_0 ($\times 10^{-3}$)	a	b	c	y	B	B'
PAW + w (this work)	20.7484	0.28318	0.59403	0.49337	0.00971	142.3	5.0
PAW + wt (this work)	20.1012	0.28014	0.58821	0.48795	0.00972	142.5	5.0
FPLAPW [24]	20.38	N/A	N/A	N/A	N/A	149	N/A
FPLMTO [3]	20.67	0.2845	0.5818	0.4996	0.01025	133.0	5.4
Experiments [2,3]	20.5815	0.28444	0.58689	0.49316	0.010242	135.5	3.8

6p electrons in the α phase are relatively deep into the core and not valence electrons; this is also true for β and γ phases. This distribution indicates that inclusion up to 6s and 6p electrons, as the default of the PAW potential in the VASP package, is sufficient. Among all electrons, the f-electrons dominate near the Fermi energy E_F. The dominance of f-electrons applies to all the three phases (α, β and γ), as shown in Fig. 4.

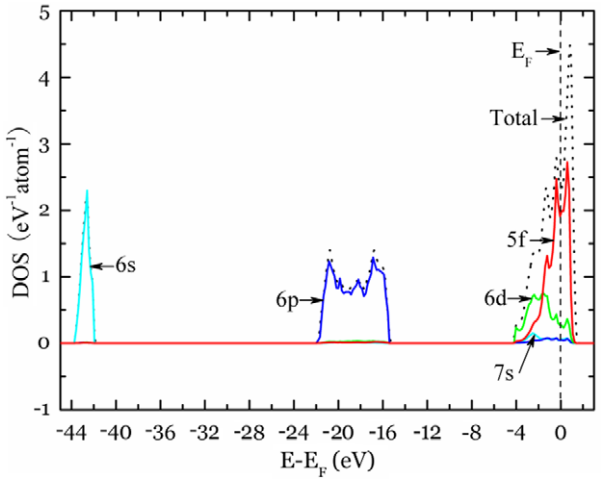

Fig. 3. Partial and total densities of state (DOS) in the equilibrium α phase as a function of energy E; based on calculations without spin–orbit interactions. Labeled are 5f, 6s, 6p, 6d, and 7s electrons and the Fermi energy E_F.

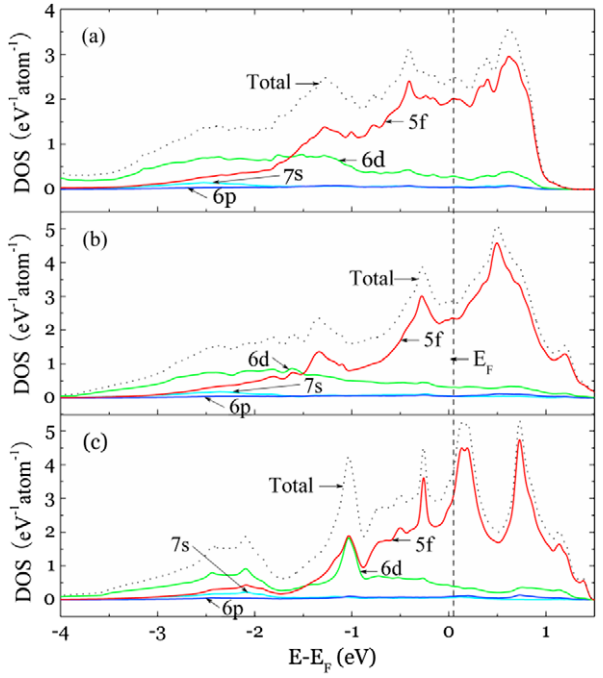

Fig. 4. Partial and total densities of state (DOS) in (a) α, (b) β, and (c) γ phases as a function of energy E; based on calculations without spin–orbit interactions. Labeled are 5f, 6s, 6p, 6d, and 7s electrons and the Fermi energy E_F.

From the distribution of electrons in energy space (that is DOS), we now turn to the distribution in real space. For clear visualization, we use contours of electron density difference (EDD). The difference is between the self-consistent electron density of the crystal, with or without defect, and the total electron density from all neutral atoms, as in [25]. Focusing on electron distribution between nearest neighbors, we plot the contours on representative high-symmetry and high-atom-density planes. In all cases, 10 zones of density difference are shown. The lightest (green for color online) zone corresponds 50 e/nm^3 or larger, and the darkest (blue for color online) –350 e/nm^3 or smaller. The other eight zones are between 50 e/nm^3 and −350 e/nm^3 with equal spacing of 50 e/nm^3. Solid lines delineate the boundaries of these zones.

Shown in Fig. 5 are EDD contours of the α, β and γ phases of U crystal. In the α phase, there is a substantial increase of electron density, relative to the total electron density from all neutral atoms, between two nearest neighbors G and J (or F and J); Fig. 5(a). This shows that there is strong orientation-dependent bonding between G and J. In contrast, the increase of electron density between nearest neighbors H and L is much less prominent, and the overall variation of electron density is more isotropic in the γ phase; Fig. 5(c). The variation of electron density in the β phases is in between those in the α and γ phases. The highly anisotropic variation of electron density in the α phase correlates with its low symmetry of crystal structure. For reference in presenting the electronic structure around Nb interstitial, we have also included the electron distribution on {1 0 0} plane; Fig. 5(d).

Having established the electron distribution in a perfect U crystal, we now turn to the focus of this study: defects in the γ phase of U. First, we examine an intrinsic defect – single vacancy – in this phase. Our calculations show that the formation energy a single vacancy in the γ phase of U is 1.08 eV. At the melting temperature of 1407 K, the fractional concentration of vacancy $e^{-1.08/kT}$ is close to 10^{-4}; here kT is the Boltzmann factor. This concentration is comparable to that of typical metals such as Cu and Al [26]. As expected, electron density near the vacancy decreases, relative to the total electron density from all neutral atoms; Fig. 6. The first nearest neighbors (such as H) relax toward the vacancy by 0.0181 nm, while the second nearest neighbors (such as D) relax outward by 0.0100 nm. As a result of the relaxation, the electron density along one close-packed direction (such as HC) decreases, and that along another (such as HD) changes little; all relative to that in perfect crystal, Fig. 5(c).

Before presenting Nb defects in the γ phase of U, we first present the results of a perfect crystal of bcc Nb. In a relaxed perfect crystal at 0 K and zero pressure, the total energy of Nb is −10.062 eV/atom. The corresponding lattice constant of the bcc structure is 0.3324 nm, which compares well with the experimental value [4] of 0.33 nm at room temperature and atmosphere pressure. This lattice

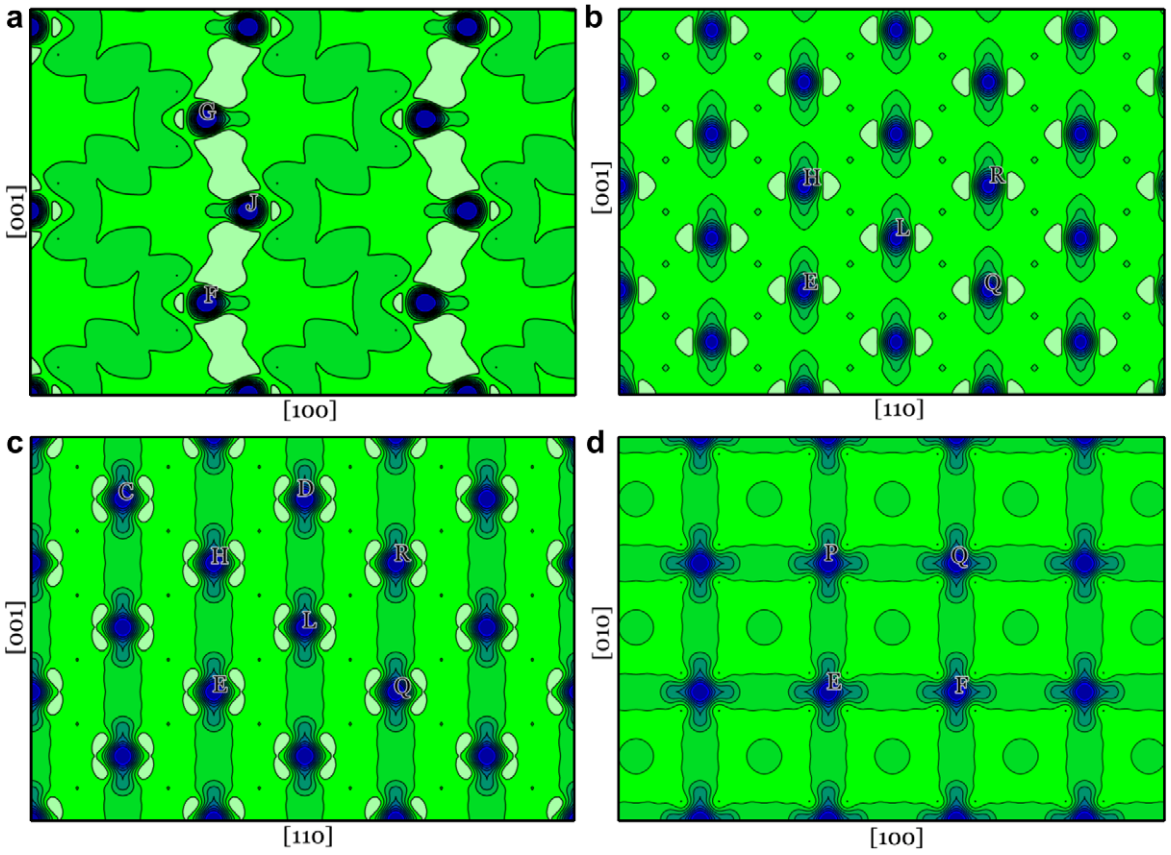

Fig. 5. Contours of electron density difference (EDD) on a (a) {110} in the α (b) {110} in the β (c) {110} in the γ, and (d) {100} in the γ phase.

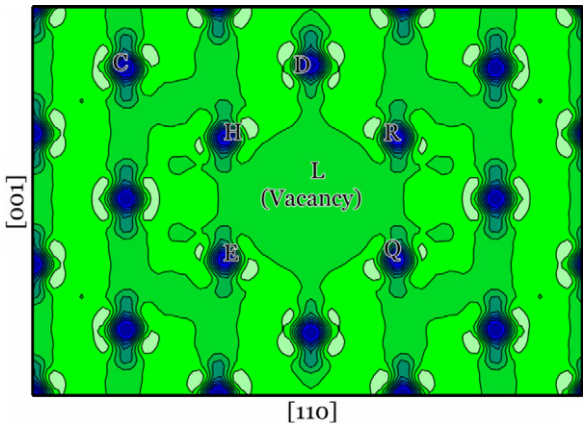

Fig. 6. Contours of electron density difference (EDD) on a {110} in the γ phase, with a vacancy in the middle.

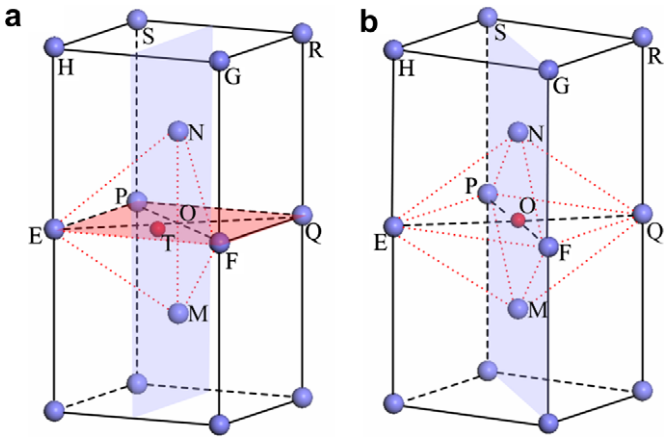

Fig. 7. Atomic configurations near (a) a tetrahedral (T) and (b) an octahedral (O) interstitial site in the γ phase of U.

constant is only a little smaller than the one of the bcc U (0.3434 nm).

In terms of Nb defects in the γ phase of U, we consider three possibilities: Nb substitution, Nb interstitial at a tetrahedral site, and Nb interstitial at an octahedral site. The tetrahedral (T) and the octahedral (O) sites are shown in Fig. 7; labels of lattice sites follow the same notations of Fig. 1. The tetrahedral site T is at the center of a tetrahedron EFMN, as shown in Fig. 7(a); on the {001} plane PEFQ, it is equal distant to points E and F, and also equal distant to point O and line EF. The octahedral site O is at the center of an octahedron EFMNPQ; it is also at the center of a {001} plane PEFQ and the center of {110} plane FMNP, as shown in Fig. 7(b). Our calculations show that the formation energy of an Nb substitution is 0.59 eV, that of Nb interstitial at the tetrahedral site 1.58 eV, and that of Nb interstitial at the octahedral site 2.35 eV. The energies correlate with the perturbations of electron density upon the formation of Nb defects.

As shown in Fig. 8, the perturbation to electron distribution increases in the order of Nb substitution, Nb interstitial at tetrahedral site, and Nb interstitial at octahedral site; relative to those in perfect crystal, Figs. 5(c) and (d). This trend is also consistent with the magnitude of ion displacements around these three defects. Near an Nb substitution, its first nearest neighbors (such as H) relax outward by 0.0049 nm, and its second nearest neighbors (such as D) relax inward by 0.0046 nm. Near an Nb interstitial at tetrahedral site, its first nearest neighbors (such as E) relax outward by 0.0368 nm, and its second nearest neighbors (not shown in Fig. 8(b)) relax outward by 0.0269 nm. Near an Nb interstitial at octahedral site, its first nearest neighbors (such as M) relax outward by 0.0843 nm, and its second nearest neighbors (such as P) relax outward by 0.0369 nm.

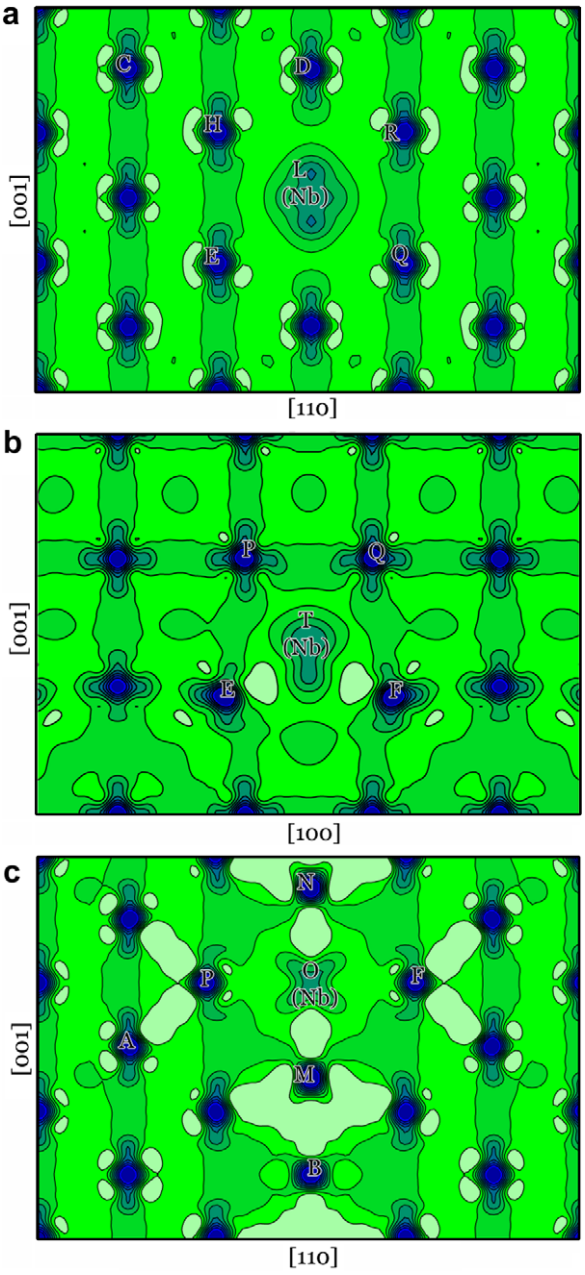

Fig. 8. Contours of electron density difference (EDD) on a (a) {110} in the γ phase of U containing a substitution Nb atom, (b) {110} in the γ phase of U containing an interstitial Nb atom at tetrahedral site, and (c) {100} in the γ phase of U containing an interstitial Nb atom at octahedral site.

4. Conclusions

In summary, we have investigated the three phases of U perfect crystals, and defects in the γ phase of U. Our calculations show: (1) f-electrons dominate the population near the Fermi energy of all phases of U perfect crystal; (2) formation energies of single vacancy, Nb substitution, Nb interstitial at tetrahedral site, and Nb interstitial at octahedral site in the γ phase of U are 1.08 eV, 0.59 eV, 1.58 eV, and 2.35 eV, respectively; (3) electron density distribution changes less near a substitutional Nb than near an interstitial Nb atom, and such changes correlates with variations of formation energies. Based on the formation energies, the thermodynamically preferable site of Nb in the γ phase U is the substitutional site.

Acknowledgements

The work is carried out through primary support of Lawrence Livermore National Laboratory under the auspices of the US Department of Energy under Contract No. 7405-Eng-48. The authors S.X. and H.H. also acknowledge support of National Science Foundation through the following programs: Partnerships for Advanced Computational Structure, Distributed Terascale Facility (DTF) and Terascale Extensions: Enhancements to the Extensible Terascale Facility.

References

[1] E. Yu Tonkov, E.G. Ponyatovsky, Phase Transformations of Elements under High Pressure, CRC, Boca Raton, 2005.
[2] C.S. Yoo, H. Cynn, P. Söderlind, Phys. Rev. B 57 (1998) 10359.
[3] C.S. Barrett, M.H. Mueller, R.L. Hitterman, Phys. Rev. 129 (1963) 625.
[4] C. Kettle, Introduction to Solid State Physics, 7th Ed., Springer, New York, 1996.
[5] V. Chazel, P. Gerasimo, V. Dabouis, P. Laroche, F. Paquet, Radiat. Prot. Dosim. 105 (2003) 163.
[6] M.M. Karnowsky, R.E. Rohde, J. Nucl. Mater. 49 (1973–1974) 81.
[7] A.V. Vatulin, A.V. Morozov, V.B. Suprun, Y.I. Petrov, Y.I. Trifonov, At. Energy 100 (2006) 37.
[8] M.K. Meyer, G.L. Hofman, T.C. Wiencek, S.L. Hayes, J.L. Snelgrove, J. Nucl. Mater. 299 (2001) 175.
[9] J. Zhou, L.M. Hsiung, J. Mater. Res. 21 (2006) 013523.
[10] D.W. Brown, R.E. Hackenberg, D.F. Teter, M.A. Bourke, D. Thomas, Los Alamos Sci. 30 (2006) 78.
[11] P. Söderlind, Adv. Phys. 47 (1998) 959.
[12] M.D. Jones, J.C. Boettger, R.C. Albers, D.J. Singh, Phys. Rev. B 61 (2000) 4644.
[13] P. Söderlind, Phys. Rev. B 66 (2002) 085113.
[14] L. Fast, O. Eriksson, B. Johansson, J.M. Wills, G. Straub, H. Roeder, L. Nordström, Phys. Rev. Lett. 81 (1998) 2978.
[15] M. Freyss, T. Petit, J.P. Crocombette, J. Nucl. Mater. 347 (2005) 44.

[16] E.A. Kotomin, R.W. Grimes, Y. Mastrikov, N.J. Ashley, J. Phys.: Condens. Matter 19 (2007) 106208.
[17] G. Kresse, J. Furthmüller, Phys. Rev. B 54 (1996) 11169.
[18] G. Kresse, D. Joubert, Phys. Rev. B 59 (1999) 1758.
[19] M.D. Segall, R. Shah, C.J. Pickard, M.C. Payne, Phys. Rev. B 54 (1996) 16317.
[20] J.P. Perdew, Y. Wang, Phys. Rev. B 45 (1992) 13244.
[21] M. Methfessel, A.T. Paxton, Phys. Rev. B 40 (1989) 3616.
[22] L.G. Zhou, H.C. Huang, Appl. Phys. Lett. 84 (2003) 1940.
[23] F. Birch, Phys. Rev. 71 (1947) 809.
[24] M.D. Jones, J.C. Boettger, R.C. Albers, Phys. Rev. B 61 (2000) 4644.
[25] J.M. Zuo, M. OKeeffe, P. Rez, J.C.H. Spence, Phys. Rev. Lett. 78 (1997) 4777.
[26] W. Jones, N.H. March, Non-equilibrium and Disorder Theoretical Solid State Physics, vol. 2, Dover Publications, New York, 1985.